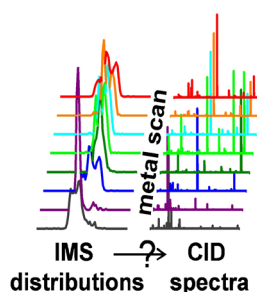**RESEARCH ARTICLE**

Populations of Metal-Glycan Structures Influence MS Fragmentation Patterns

Feifei Zhu, Matthew S. Glover, Huilin Shi, Jonathan C. Trinidad, David E. Clemmer

Department of Chemistry, Indiana University, 800 Kirkwood Ave., Bloomington, IN 47405, USA

Abstract. The structures and collision-induced dissociation (CID) fragmentation patterns of the permethylated glycan $Man_5GlcNAc_2$ are investigated by a combination of hybrid ion mobility spectrometry (IMS), mass spectrometry (MS), and MS/MS techniques. IMS analysis of eight metal-adducted glycans ($[Man_5GlcNAc_2 + M]^{2+}$, where M = Mn, Fe, Co, Ni, Cu, Mg, Ca, and Ba) shows distinct conformer patterns. These conformers appear to arise from individual metals binding at different sites on the glycan. Fragmentation studies suggest that these different binding sites influence the CID fragmentation patterns. This paper describes a series of separation, activation, and fragmentation studies that assess which fragments arise from each of the different gas-phase conformer states. Comparison of the glycan distributions formed under gentle ionization conditions with those obtained after activation of the gas-phase ions suggests that these conformer binding states also appear to exist in solution.

Keywords: Ion mobility spectrometry, Collision-induced dissociation, Metal-glycan interactions, Glycan ion structure

Introduction

Carbohydrates play many key roles in biological processes of living organisms [1–3]. One such role involves the sequester and transport of metal ions [4, 5]. Carbohydrates and associated derivatives are able to coordinate metal ions, resulting in metal–carbohydrate complexes that have improved solubility, reduced toxicity, and greater biocompatibility compared with metal complexes lacking carbohydrates [6, 7]. Although substantial progress in understanding carbohydrate structures and functions has been made, many systems remain incompletely characterized, highlighting the need for improved analytical approaches.

Mass spectrometry (MS), together with soft ionization techniques such as electrospray ionization (ESI) [8], is positioned to revolutionize the analysis of carbohydrate structures [9, 10]. In most analyses, carbohydrates are either protonated or sodiated, and there is an emerging literature detailing how the choice of charge carrier affects ionization efficiencies, fragmentation processes, and carbohydrate structures [11–

15]. Several papers have compared ionization efficiencies of underivatized glycans in the presence of various metals and demonstrated that individual metals could induce distinct fragmentation patterns during collision-induced dissociation (CID) and electron activated dissociation [16–20]. However, much less is known about the structures of carbohydrate complexes associated with different charge carriers, such as transition metals.

Another promising technique for carbohydrate analysis is ion mobility spectrometry (IMS) [21–25]. Many groups have investigated the structures of carbohydrates by combined IMS-MS methods [26–38]. IMS separates ions based on their shapes, and in combination with theoretical calculations, IMS measurements have emerged as a means of inferring information about ion structures. In particular, carbohydrates ionized with alkaline metals have shown isomer-specific and metal-specific collision cross-sections [36, 37]. Our group has used IMS to characterize mixtures of isomeric saccharides, revealing that individual isomers may exist as multiple stable conformers [39–41]. To investigate further the nature of these conformers, multidimensional IMS (IMS-IMS) [42] has been employed to examine gas-phase interconversions between structural states. These studies utilize a relatively gentle collisional activation process. That is, the activation energy for ions is adjusted so that it is sufficient to induce a sampling of a new set of conformations referred to as the gas-

Correspondence to: David E. Clemmer; *e-mail:* Clemmer@Indiana.EDU

phase quasi-equilibrium (QE) distribution [43, 44], yet still below the dissociation threshold. This technique is especially useful for determining which structures may be present in the solution phase versus which are more likely to be generated upon activation in the gas phase.

In the work described below, we investigate metal ions bound to the permethylated glycan $Man_5GlcNAc_2$ isolated from ribonuclease B. We have studied complexes involving eight divalent metal ions (Mn^{2+}, Fe^{2+}, Co^{2+}, Ni^{2+}, Cu^{2+}, Mg^{2+}, Ca^{2+}, and Ba^{2+}). A similar study involving metals binding to peptides has been reported recently [45]. In the case of peptides, it appears that transition metals bind differently than the alkaline earth metal Ca^{2+}, which is reflected in both the IMS distributions and the CID fragmentation patterns. Below, we describe experiments aimed at further understanding the relationship between IMS conformations and CID fragmentation patterns for metallated glycan species.

We choose the glycan $Man_5GlcNAc_2$ for these experiments because it is a well-studied glycan model. It has been reported to exist as a single covalent structure [46, 47], yet our current IMS analysis shows that it can exist as multiple conformations for each metallated glycan ion. Combining IMS analysis with MS/MS, we conclude that these metal-dependent features result from the metals binding the glycan at distinct sites. This differential site occupancy is responsible for the specific fragmentation events observed during CID. This approach allows us to characterize the distribution of gas-phase binding configurations, and by comparing the populations before and after activation, we are able to evaluate the populations of different metal-glycan binding states that may be present in solution.

Experimental

General

IMS theory and instrument designs have been previously reported [23, 48–55]. The IMS-(IMS-)MS analysis in this work is performed on a home-built instrument that has been described previously [43, 56, 57]. The details regarding different instrumentation components and modes of operations are reported elsewhere [42, 58], and only a brief description is provided here. The instrument is comprised of an electrospray source, a 183-cm long drift tube, and a time-of-flight mass analyzer. A TriVersa NanoMate autosampler (Advion, Ithaca, NY, USA) is used to electrospray sample solutions into the source, where ions are accumulated in an hourglass funnel [59] and periodically gated into the drift tube. The drift tube is filled with ~3 Torr helium buffer gas and operated with a drift field of ~10 V·cm^{-1}. Ions are separated through collisions with the buffer gas while migrating down the drift tube. Upon exiting the drift tube, ions are extracted and orthogonally pulsed into the time-of-flight mass analyzer. The IMS-MS dataset is collected in a nested fashion [54], which allows the drift time (t_d, ms timescale) and flight time (μs timescale) to be obtained from the same scan. The

drift time is converted into collision cross-section (Ω) using the following equation:

$$\Omega = \frac{(18\pi)^{1/2}}{16} \frac{ze}{(k_bT)^{1/2}} \left[\frac{1}{m_1} + \frac{1}{m_b}\right]^{1/2} \frac{t_dE}{L} \frac{760}{P} \frac{T}{273.2} \frac{1}{N} \quad (1)$$

where the variables E, L, T, and P correspond to the electric field, length, temperature, and pressure of the drift tube, respectively. The variable m_b refers to the mass of the buffer gas, m_I is the mass of the analyte ion, and ze is the charge of the analyte ion. The constant k_b is the Boltzmann's constant and N is the neutral number density of the buffer gas at standard temperature and pressure. The drift region contains several ion funnels and is not a strictly linear electric field. We obtain precise cross section measurements by determing the t_d of ions as they traverse between the source and middle funnel of the drift tube, a region that does possess a uniform drift field. Alternatively, we can measure the t_d of ions as they traverse the entire drift tube. In this case, cross-sections are calibrated to values measured using the aforementioned method in order to account for the nonlinear drift field inside the ion funnels.

IMS-MS Instrumentation and Measurements

Two operational modes of the instrument were utilized in this work. The source distributions of the glycan ions were obtained in IMS-MS mode, where the drift tube was operated as a uniform drift region. This home-built instrument is designed to have a gentle ionization source, which minimizes ion activation during ESI. Gas-phase ions produced during ESI have been shown to retain their distribution of solution structures [57, 60–68], and we find empirical evidence that the distribution generated at the source can preserve some characteristics of solution equilibria [57, 68].

The QE distributions were measured using IMS-IMS-MS mode, where we operated the drift tube as two independent drift regions separated by an ion funnel. In this mode, the glycan conformations corresponding to each feature in the source distribution were mobility-selected after the first drift region and collisionally activated before subsequent separation in the second drift region. The activation voltages for reaching QE distributions for different metal-glycan ions varied from 130 to 190 V.

MS/MS Measurements

The CID experiments were performed separately on an LTQ Velos instrument (Thermo Scientific, San Jose, CA, USA), which is part of a home-built hybrid instrument that has been previously described [40, 69, 70]. This instrument contains a source region that is essentially identical to the one used in the IMS-MS measurements. This ensures sampling of nearly identical ion populations during ESI on these two instruments. The isolated precursors were fragmented in the linear ion trap under

a resonant rf excitation waveform applied for 10 ms with 38% normalized collision energy and an activation q of 0.25.

Materials

Ribonuclease B from bovine pancreas, peptide:*N*-glycosidase F (PNGase F), chloroform, NaOH beads (97% purity), iodomethane, 2-mercaptoethanol, acetonitrile (ACN), and all metal acetates were purchased from Sigma-Aldrich (St. Louis, MO, USA). C18 micro-spin columns and empty micro-spin columns were from Harvard Apparatus (Holliston, MA, USA). Water (HPLC grade) was obtained from EMD Chemicals (Darmstadt, Germany). Dimethylformamide (DMF), trifluoroacetic acid (TFA), and formic acid were obtained from Mallinckrodt Baker (Phillipsburg, NJ, USA).

Sample Preparation

A detailed procedure of glycan purification and permethylation has been published elsewhere [71]. Briefly, 100 μL of ribonuclease B solution (1 mg·mL^{-1} in 10 mM sodium phosphate buffer and 0.1% 2-mercaptoethanol at pH 7.5) was denatured at 95°C for 5 min. After the solution was cooled to room temperature, 0.5 μL of PNGase F (500 mu·mL^{-1}) was added followed by overnight incubation at 37°C. The digest was then diluted with 100 μL of aqueous solution containing 5% ACN and 0.1% TFA before being purified using a C18 micro-spin column. After preconditioning the column with 400 μL of 85% ACN and 0.1% TFA, the digest was loaded three times onto the micro-spin column. The collected solution was dried using a vacuum centrifugal concentrator (Labconco Corp., Kansas, MO, USA) for subsequent permethylation. The permethylation was performed using the spin-column method described elsewhere [71]. An empty column was packed with NaOH beads (suspended in ACN) up to 1 cm from the top of the column and then preconditioned with DMF. The dried glycan mixture was reconstituted with 45 μL of iodomethane, 60 μL of DMF, and 2.4 μL of water and mixed briefly. The reaction mixture was loaded onto the column and incubated for 15 min before centrifugation. After the second addition of 45 μL of iodomethane, the mixture was reloaded onto the column and incubated for another 15 min. The column was then washed with two applications of 50 μL of ACN. The permethylated glycans were extracted with 400 μL of chloroform and dried under vacuum. The dried glycans were dissolved in the electrospray solution comprised of 49.9:49.9:0.2 (v:v:v) water:ACN:formic acid and 10 mM metal acetate.

Data Analysis

The intensities of the three major CID fragments and the peak areas of the three major IMS conformers (see below for details) were determined for comparison. For these calculations, all fragments above 1% relative intensity in the CID spectrum were measured and normalized to the total fragment ion intensity. The normalized intensity of each major fragment was the summed intensity of the singly- and doubly charged ions as well as the corresponding water loss peak if observed. The peak area of each major conformation in the QE distribution was obtained by integrating the signal of the peak associated with the corresponding cross section range and normalizing by the total area. To quantitatively compare metal-binding behaviors, Pearson correlation coefficient (PCC) was calculated for each pair of metal-adducted glycans. The PCC for CID fragmentation patterns was calculated based on all major and minor fragments above 1% relative intensity, and for QE distributions, the value was calculated based on the cross section distribution from 300 to 360 Å^2 (see below for details). A perfect positive linear correlation between the two variables would give a PCC value of 1.0, while a value of –1.0 would indicate these values are completely anti-correlated. A value of 0 would indicate that the two variables are uncorrelated.

Results and Discussion

Source Distributions of the [Man$_5$GlcNAc$_2$ + M]$^{2+}$ Ions

The black traces in Fig. 1 show the cross section distributions of metal-adducted Man$_5$GlcNAc$_2$ ions generated at the ESI source region, which we refer as the "source distributions." Our lab has previously demonstrated that the distribution of structural conformations obtained under mild ionization conditions often preserves the population of solution phase structures [52, 57, 68]. These distributions show distinctive features, having cross-sections ranging from 310 to 350 Å^2. For example, the [Man$_5$GlcNAc$_2$ + Mn]$^{2+}$ ion shows three main peaks at 318, 341, and 347 Å^2. While the first peak at 318 Å^2 is well resolved, those at 347 and 341 Å^2 are only partially separated from each other. Metal-glycan adducts involving Fe^{2+} and Co^{2+} metals exhibit similar distributions. The main peaks are centered at 341 Å^2. Two smaller peaks centered at 319 and 331 Å^2 are observed with lower intensities (<30% of the main peak). The cross-section distribution of [Man$_5$GlcNAc$_2$ + Ni]$^{2+}$ is similar to that of the Mn^{2+} adducted glycan ions; however, an additional shoulder to the left of the 341 Å^2 peak is observed (Fig. 1). The Cu^{2+} adducted glycan ions display a distribution that is distinct from the rest of the transition metal adducts. No peak is observed around 318 Å^2 (Fig. 1). Instead, the ions display a broad distribution from 327 to 347 Å^2 with three partially resolved conformations at 335, 341, and 345 Å^2.

The cross-section distribution of [Man$_5$GlcNAc$_2$ + Mg]$^{2+}$ shows two main peaks at 317 and 341 Å^2 (Fig. 1). This pattern of features is more similar to that observed for the transition metal ion adducts (i.e., Mn^{2+}, Fe^{2+}, Co^{2+}, Ni^{2+}, and Cu^{2+}) than it is to the alkaline earth metals (i.e., Ca^{2+} and Ba^{2+}), presumably because the ionic radius of Mg^{2+} is similar to those of transition metals (Table 1). Compared with Mg^{2+}, different features are observed for the Ca^{2+} and Ba^{2+} adducted glycan ions. The Man$_5$GlcNAc$_2$ + Ca]$^{2+}$ ion shows at least four peaks centered at 321, 329, 337, and 342 Å^2 (Fig. 1). The two peaks
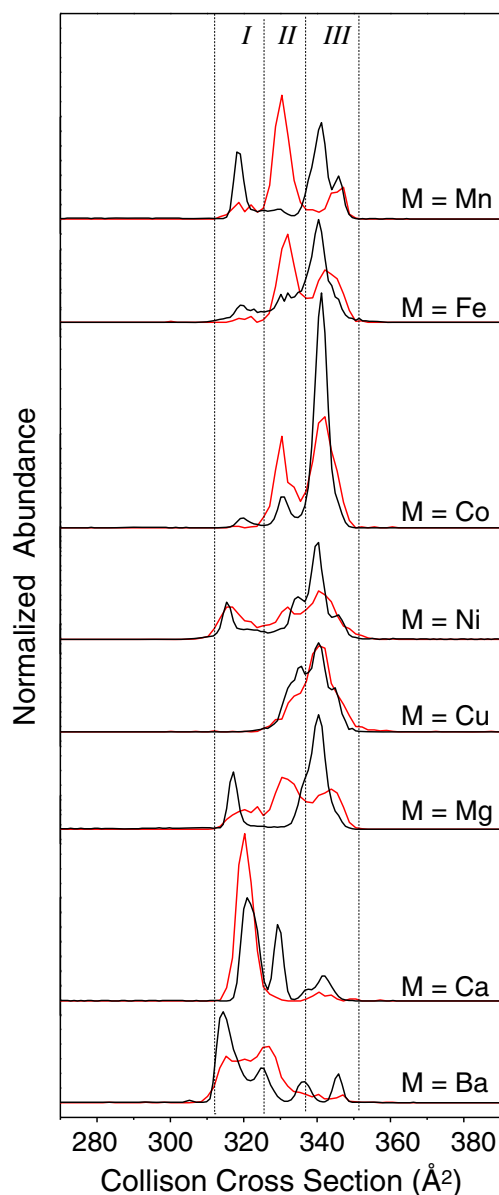
Figure 1. Source distributions (black traces) and quasi-equilibrium distributions (red traces) of metal-adducted $Man_5GlcNAc_2$ glycan ions plotted on a cross section scale. Each panel corresponds to the distribution of the $[Man_5GlcNAc_2 + M]^{2+}$ glycan ion, where M refers to the divalent metals of Mn, Fe, Co, Ni, Cu, Mg, Ca, and Ba, as shown on each panel. The dashed lines divide the distributions into three cross-section ranges labeled as *I*, *II*, and *III* based on their quasi-equilibrium (QE) distributions. The distributions are obtained by integration of the drift bins across a narrow *m/z* range corresponding to each of the glycan ions and normalized to the total ion abundance

For both Ca^{2+} and Ba^{2+} adducted glycan ions, the peak with the smallest cross-section gives the highest intensity. It is interesting to note that despite the much larger ionic radius of Ba^{2+} (Table 1), the most intense feature (314 $Å^2$) in the distribution has a smaller cross-section than that of Ca^{2+} (321 $Å^2$) (Fig. 1). Similar observations for alkaline metal-adducted saccharides have also been reported [36, 37]. These observations seem to suggest that the overall size of a metallated carbohydrate depends not only on the ionic radius of the metal ion but also the preferred coordination of the metal combined with the structural flexibility of specific carbohydrate moieties [18]. In our case, the smaller cross-section suggests that Ba^{2+} may adopt a higher coordination number than Ca^{2+}, resulting in tighter overall binding with the glycan.

CID of the $[Man_5GlcNAc_2 + M]^{2+}$ Ions

Figure 2 shows the CID spectra for each of the $[Man_5GlcNAc_2 + M]^{2+}$ ions. The fragments were assigned with the assistance of online software GlycoWorkBench [72] and labeled according to the Domon and Costello nomenclature [73]. The observed fragments result predominantly from glycosidic cleavages and appear either singly- or doubly charged. In the singly charged cases, these occur because of loss of a proton with retention of the metal ion. Regardless of which metal ion is adducted, fragmentation mainly occurs at three sites: the GlcNAc1-4GlcNAc bond at the reducing terminus that yields the B_4 fragment; the Man1-6Man bond at the branching site that gives the $Y_{3\alpha}$ fragment; and one of the three Man–Man bonds at the non-reducing terminus. Such a cleavage at the non-reducing terminus can result in three types of fragments: $Y_{3\beta}$, $Y_{4\alpha'}$, and $Y_{4\alpha''}$ (Scheme 1). These three fragments have the same mass and are thus indistinguishable from each other in MS. For succinctness, "$Y_{3,4}$" is used here to represent these three types of fragments in the following discussions. Detection of specific fragments that retain the metal ion allows one to deduce the possible metal-binding sites on the adducted parent glycan. This is similar to how fragmentation spectra of peptides have been used to localize adducts on parent structures [45, 74, 75]. A number of minor fragments are also produced during CID (e.g., the Y_1 fragment in the spectrum of the Ni^{2+} adducted glycan ion); however, the intensities of these fragments are below 3% of the total fragment intensity.

The singly charged (metal-adducted) $Y_{3\alpha}$ fragment is the base peak in the CID spectra of the Mn^{2+}, Fe^{2+}, Co^{2+}, and Mg^{2+} adducted glycan ions (Fig. 2), indicating that these metal ions are predominantly localized at the branching mannose site. The $Y_{3,4}$ ions (singly- and doubly charged), are the second most abundant fragment ions for these metallated species, whereas B_4 ions are the third most abundant. Some fragment ions apparently result from the loss of two terminal residues, e.g., the $B_4/Y_{3,4}$ ions. Similar types of fragments have previously been observed in CID spectra [14, 76]. It is likely that these fragments are produced in a cooperative fashion [77, 78] but the exact pathway is not clear. The CID spectra of Mn^{2+} and Mg^{2+} adducted glycan ions have similar fragmentation patterns

with larger cross-sections at 337 and 342 $Å^2$ have smaller intensities and are only partially separated from each other. In a similar pattern, four peaks are observed for the $[Man_5GlcNAc_2 + Ba]^{2+}$ ion, with cross-sections at 314, 325, 336, and 346 $Å^2$. In this case, the two peaks having smaller cross-sections at 314 and 325 $Å^2$ are only partially separated.

Table 1. Estimated Populations of the Metal-Binding Sites on the Glycan $Man_5GlcNAc_2$ in the Source and QE Distributions

Metal type	Ionic radii[a] (pm)		Percentage					
			Source distribution			Quasi-equilibrium distributions		
	CN[b] = 4	CN = 6	Reducing terminus	Branching site	Non-reducing terminus	Reducing terminus	Branching site	Non-reducing terminus
Mn^{2+}	66	83	27	14	60	12	66	22
Fe^{2+}	63	61	13	31	56	5	56	39
Co^{2+}	56	65	4	15	81	2	44	54
Ni^{2+}	49	69	20	28	51	33	26	41
Cu^{2+}	57	73	4	41	55	2	32	66
Mg^{2+}	57	72	21	18	60	23	44	33
Ca^{2+}	–	100	53	33	15	95	2	3
Ba^{2+}	–	135	–	–	–	–-	–	–

[a]Ionic radii are recorded from the CRC Handbook of Chemistry and Physics, 94th edition, 2013–2014.
[b]CN = coordination number.

at the mass range of $400-800\,m/z$. Within this range, the predominant fragments are doubly charged versions of $Y_{3,4}$, B_4, and $Y_{3\alpha}$ as well as secondary fragmentations of these species. In contrast, Fe^{2+} and Co^{2+} adducted glycan ions show different fragment patterns in the $400–800\,m/z$ mass range, where the intensities of the doubly charged $Y_{3\alpha}$ and B_4 ions are extremely low. For the Cu^{2+} adducted glycan, the $Y_{3,4}$ ion is the most intense fragment in the spectrum, suggesting that Cu^{2+} prefers to bind to the non-reducing terminus of the glycan structure. The singly charged $Y_{3\alpha}$ and B_4 fragments are the second and third most abundant product ions, respectively.

The $[Man_5GlcNAc_2 + Ni]^{2+}$ ion produces a quite different fragment spectrum compared with the rest of the transition metal adducts (Fig. 2). In contrast to the previous cases where a metallated fragment ion is the most abundant species, in the case of Ni^{2+}, the protonated B_4 ion is the base peak, despite the fact that the precursor ion is not protonated. Similar examples of protonated fragment ions have been observed during CID of metallated peptides [79, 80] and carbohydrates [17, 19]. The exact mechanism for the formation of these protonated species has not been established. However, it is proposed that during fragmentation, the B_4 fragment abstracts a proton from the resulting Y_1 ion. For the Ni^{2+} adducted glycan, all three fragments ($Y_{3,4}$, B_4, and $Y_{3\alpha}$) are present as intense peaks in the CID spectrum, which indicates that Ni^{2+} binds to multiple sites on the glycan structure.

The CID spectra of Ca^{2+} and Ba^{2+} adducted glycan ions are very similar (Fig. 2). In both cases, the doubly charged B_4 ion is the most abundant peak, suggesting that a high percentage of Ca^{2+} and Ba^{2+} ions are located at the reducing terminus of the glycan structure. The singly charged fragments are much less abundant relative to those for the transition metal adducts, an effect that is even more pronounced in the case of Ba^{2+}. Comparisons of the fragmentation spectra show that Mg^{2+} behaves more like the transition metals than the alkaline earth metals of Ca^{2+} and Ba^{2+}, a similarity that has also been noted for the source distributions of the metallated glycans (Fig. 1).

Because the location of metal ion binding may direct glycan fragmentation, determining the similarity between fragment ion abundances across the series of metal ions would allow

us to determine which sets of metal ions bind to the glycan in a similar fashion. For each pair of metal ions, we calculated the Pearson correlation coefficient (PCC) using the relative abundances from the major and minor fragment ions (Supplementary Table S1). The fragmentation patterns for Mg^{2+}, Mn^{2+}, Fe^{2+}, and Co^{2+} are extremely similar, with correlations between 0.96 and 0.99. This implies that these four metal ions bind to the glycan in very similar manner. In contrast, the fragmentation pattern for Ba^{2+} does not correlate at all with those of the transition metals, with values ranging from –0.08 to 0.03, in agreement with our observation that Ba^{2+} adducts possess a distinct range of conformations in the source distribution. However, Ba^{2+} shows a PCC value of 0.96 with Ca^{2+}, indicating that these two alkaline earth metals bind to the glycan with similar distributions.

Quasi-Equilibrium Distributions of the $[Man_5GlcNAc_2 + M]^{2+}$ Ions

Although we observe clear correlations between the fragmentation patterns of sets of metal ions, the similarities are not as striking when we examine their respective source distributions. We hypothesize that the source distributions of the metal-adducted glycan ions do not represent the actual populations of conformations from which CID fragments are produced. In the initial phase of CID, the glycans are collisionally activated, which is similar to (albeit stronger than) the activation used to reach the QE distribution. We therefore examined the QE distributions of the metallated glycan ions (Fig. 1, red traces). The QE distribution is obtained by mobility-selecting a conformer formed in the source distribution and activating it in a high electric field region. Regardless of which source conformation is selected for a given glycan ion, a nearly identical QE distribution is obtained upon collisional activation (an example is shown in Supplementary Figure S1). Activation in this fashion allows ions to overcome energy barriers between different conformational states, enabling the system to repopulate as a function of the relative energy levels of different gas-phase conformations. Thus, an additional merit of this technique is the ability to distinguish whether a set of peaks in the IMS
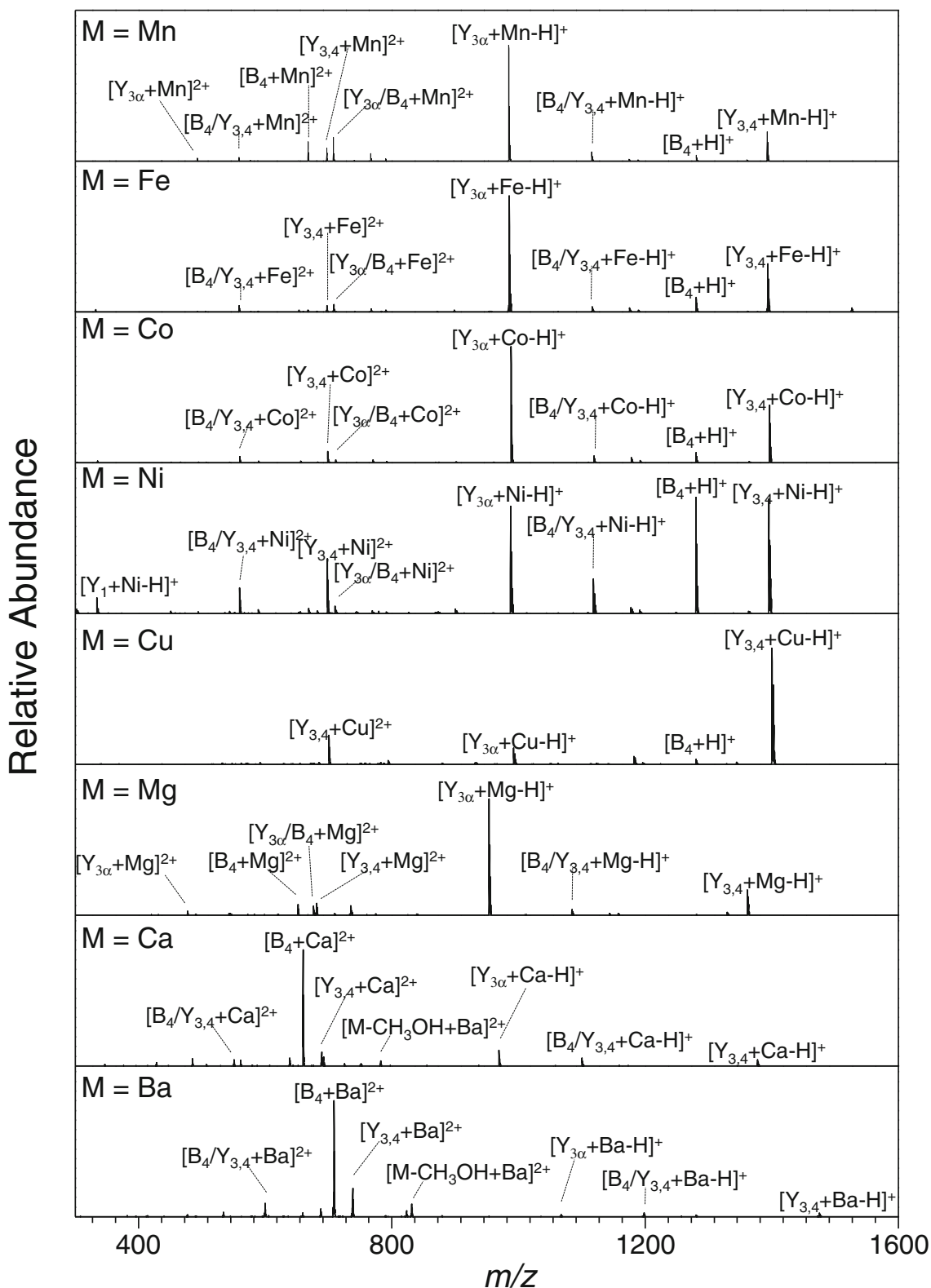
Figure 2. CID spectra of the $[Man_5GlcNAc_2 + M]^{2+}$ glycan ions. The fragment ions, either doubly charged or singly charged, are predominantly formed by glycosidic cleavages at the B_4, $Y_{3\alpha}$, and $Y_{3,4}$ positions of the glycan structure

distribution belongs to multiple gas-phase conformations of a single isomer or, instead, to multiple isomers. In the former case, activation of individual IMS peaks would result in the same QE distribution, whereas in the latter case, different QE distributions will be obtained after activation [81]. Different isomeric structures are not expected to reach the same QE
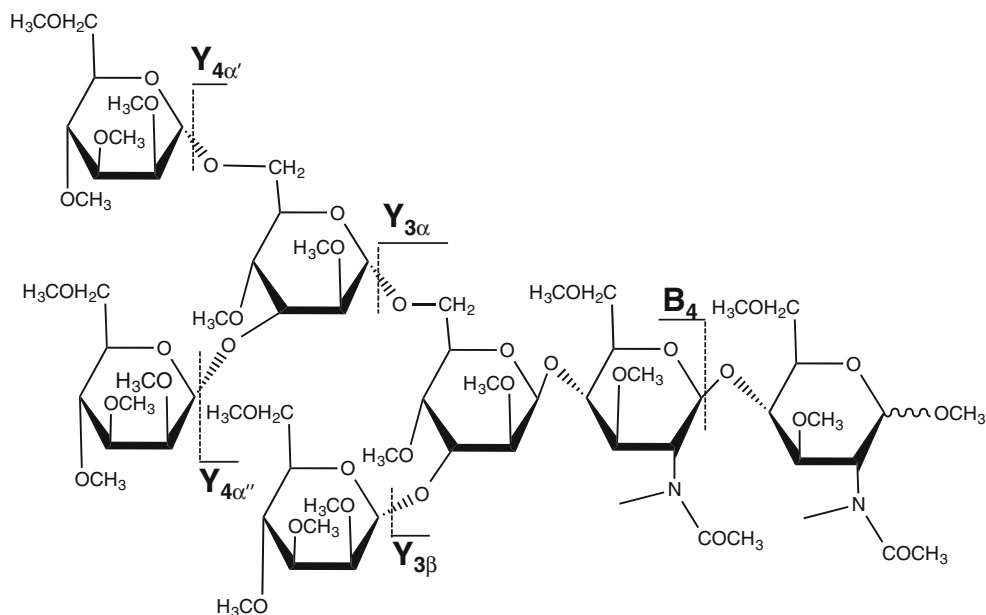
Scheme 1. Structure of the permethylated $Man_5GlcNAc_2$ glycan showing the major fragments observed in the collision-induced dissociation (CID) spectra. Cleavages at the non-reducing terminal mannoses lead to three possible fragments $Y_{4\alpha'}$, $Y_{4\alpha''}$, and $Y_{3\beta}$ that are indistinguishable from each other. For succinctness, "$Y_{3,4}$" is used to refer to any of these three types of fragments

distribution because this would involve bond breakage and reformation, which is unlikely to occur under gentle activation conditions. Our observation that the set of peaks in the IMS distribution for a given metal-glycan ion could reach the same QE distribution supports the view that the $Man_5GlcNAc_2$ glycan has only a single covalent structure.

The QE distributions of the metal-adducted glycan ions exhibit three main conformations labeled as *I*, *II*, and *III* (Fig. 1), having the cross section ranges of 308–324, 324–337, and 337–350 Å^2, respectively. In the case of the Mn^{2+} adducted glycan ion, conformer *II* is the highest intensity feature followed by conformer *III* and then *I*. The Mg^{2+} adducted glycan ion shows a similar trend, although the three conformations are largely unresolved. The QE distributions of $[Man_5GlcNAc_2 + Fe]^{2+}$ and $[Man_5GlcNAc_2 + Co]^{2+}$ both contain conformers *II* and *III*, with a slight difference in the intensity ratios (Fig. 1). Conformer *I* is at very low abundance in the case of either metal. Conformation *III* is the primary conformation for Cu^{2+} adducted glycans. Conformer *II* shows up as a minor conformation partially separated from conformer *III*, displaying a left shoulder from the main peak. Essentially no conformer *I* is observed for the Cu^{2+} adducted glycan. The QE distribution of the Ni^{2+} adducted glycan ion is very broad, and the three conformations are partially separated (Fig. 1). The distribution differs from the other transition metals in that conformers *I*, *II*, and *III* are present in approximately equal amount.

The glycans adducted with alkaline earth metals Ca^{2+} and Ba^{2+} show QE distributions that are markedly different from the rest of the metals. In the case of $[Man_5GlcNAc_2 + Ca]^{2+}$, conformer *I* is the most abundant (Fig. 1). Conformer *III* shows

up as a minor feature that is much less intense, whereas conformer *II* is almost nonexistent. The Ba^{2+} adducted glycan ion exhibits a very broad distribution, and for this metal, conformers *I* and *II* overlap with each other (Fig. 1). In contrast, conformer *III* is much less abundant. It is interesting to observe that although Ca^{2+} and Ba^{2+} have much larger ionic radii than the rest of the metals, the stable gas-phase conformers favor smaller cross sections, an observation also noted for the source distributions.

Similar to the situation during MS/MS fragmentation, the QE distribution also appears to be influenced by the distribution of metal-binding locations on the glycan. Therefore, if sets of metal ions show similar QE distributions, this would indicate that these metal ions bind to the glycan at a similar distribution of sites. For each pair of metal ions, we calculated the PCC of their QE distributions (Supplementary Table S2). The QE distribution for Mg^{2+} is very similar to those of Mn^{2+}, Fe^{2+} and Co^{2+}, with a PCC range from 0.74 to 0.91; however, these metals are poorly correlated with Ba^{2+} (with a range from –0.14 to 0.25). The QE distribution most similar to Ba^{2+} is that of Ca^{2+}, with a value of 0.53.

The correlation analysis of both the MS/MS and QE data allows two independent approaches to group metal ions based on similar glycan binding characteristics. If the hypothesis that the QE conformations represent the intermediates along the MS/MS pathway is correct, the PCC calculations from both approaches should agree with each other. To quantitatively compare the results of both analyses, we plotted the PCC values from the MS/MS analysis as a function of the PCC values from the QE analysis, with the results shown in Fig. 3. There appears to be a linear relationship between these two
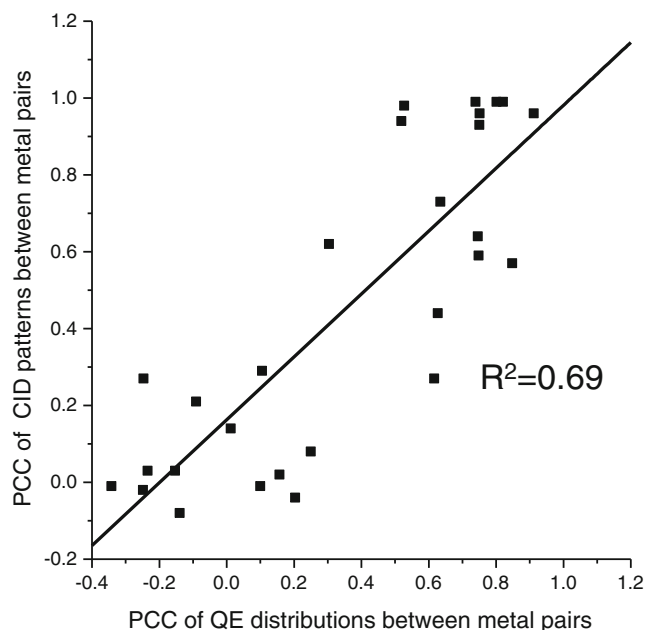
Figure 3. The scatter plot shows the correlations between metal-dependent QE conformations and metal-dependent CID fragmentation patterns. Each data point contains the calculated Pearson correlation coefficients for each pair of metals based on their CID fragmentation patterns (*y* value) and QE distribution patterns (*x* value)

datasets ($R^2 = 0.69$), suggesting that for metal-glycans that are structurally alike (i.e., having similar QE distributions), they also have the tendency to produce similar fragmentation patterns. This observation indicates that MS/MS fragmentation patterns result from a distribution of gas-phase conformations that are similar, if not identical to the QE distributions.

Correlating the IMS Features with the Binding Positions of the Metal Ions

The above analysis demonstrates a correlation between the QE distribution and the fragmentation pattern for a given glycan ion. In order to uncover the nature of such a relationship, the

intensities of the three major fragments and QE peak areas of the three conformers are plotted in Fig. 4.

Figure 4 reveals that the abundances of conformers *I*, *II*, and *III* from the QE distributions correlate strongly with the intensities of fragment ion B_4, $Y_{3\alpha}$, and $Y_{3,4}$, respectively. For example, the Mn^{2+} adducted glycan produces the B_4, $Y_{3\alpha}$, and $Y_{3,4}$ fragment ions at a 0.2:1:0.3 ratio. This is essentially identical to the ratio that is observed for conformers *I*, *II*, and *III* (Fig. 4). Conformer *II* is the most abundant peak in the QE distribution, and fragment ion $Y_{3\alpha}$ is most intense in the MS/MS spectrum. Conformer *III* is the second most abundant, and fragment ion $Y_{3,4}$ is the second most intense in the MS/MS spectrum. Similar correlations between the QE distributions and the fragmentation patterns are observed for nearly all metals ions (Fig. 4). The same data from the bar graphs are also presented in the scatter plot (Supplementary Figure S2), which shows nearly linear dependences for the three pairs of CID fragments and QE conformers.

The largest outlier from this trend is the Ba^{2+} adducted glycan ion, for which conformer *II* shows a higher abundance than conformer *III*. This does not correlate well with the observed fragment intensities. We propose that this discrepancy may result from the fact that Ba^{2+} has a much larger ionic radius than the rest of the metals. The QE distribution of $[Man_5GlcNAc_2 + Ba]^{2+}$ (Fig. 1) shows that conformer *I* has a very extended distribution, which is almost inseparable from that of conformer *II*. Our analysis has used the same fixed range of cross sections for each glycan ion to define a given conformation. However, Ba^{2+} has a significantly larger ionic radius than the other metals (Table 1), which may have resulted in an underestimation of conformer *I* and a corresponding overestimation of conformer *II*. The actual conformer abundances may be more consistent with those determined from the fragmentation spectrum. Along those lines, while we observe three main features in the QE distributions, the total number of unique conformers can be greater. Minor QE conformations may be present that overlap with these three conformations, and these minor conformations may be the source of the minor fragments in the CID spectra. However, if additional QE conformations exist, they are likely to be at relatively low abundances because
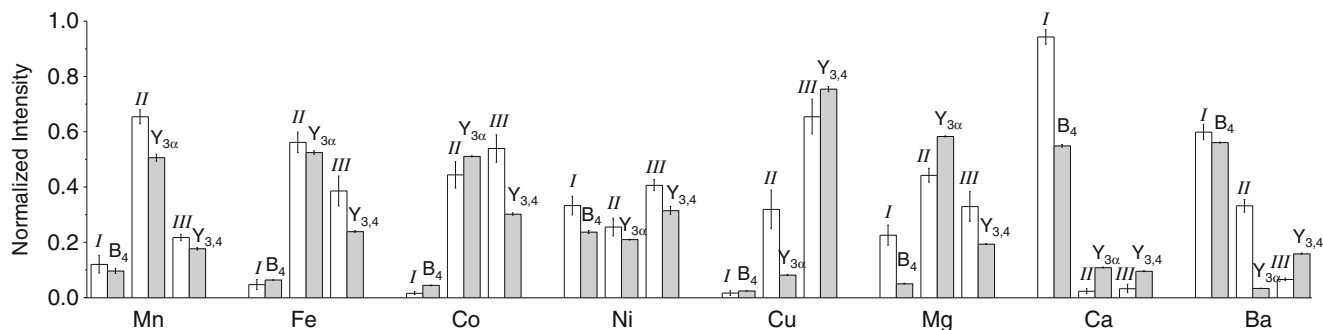

Figure 4. The bar graphs show the comparisons between the peak areas of the three conformations from QE distributions (white bars, representing conformers *I*, *II*, and *III*, from left to right) and the intensities of the three major fragments (grey bars, representing fragments B_4, $Y_{3\alpha}$, and $Y_{3,4}$, from left to right) for each metallated glycan. Error bars show the standard deviations from triplicate measurements

the minor CID fragments account for only between 6% (for Cu^{2+}) and 24% (for Ca^{2+}) of the total fragment ion intensity.

Based on the correlation between QE distributions and fragment patterns, we propose that during the initial stages of CID fragmentation, collisions with buffer gas result in a redistribution of glycan conformations similar to that observed during the activation in the IMS-IMS-MS mode to yield the QE distribution. This phenomenon has been observed for metallated peptides previously in our laboratory [45]. During activation, the short (3 mm) activation region contains a high electric field (up to 700 V/cm for this study). Ions are accelerated and, upon collisions with the buffer gas, the ions are imparted with sufficient energy to overcome the barriers between different conformations. This is very similar to the energy transfer process in CID [82–84] However, in contrast to CID, collisional activation under the QE condition does not result in significant ion fragmentation. From the underlying QE distribution, the relative fragment ion intensities can be predicted. The population in the QE distribution is a function of the conformational energy landscape in the gas phase and provides insight into the binding preferences of metals on the glycan.

As has been described above, the B_4, $Y_{3\alpha}$, and $Y_{3,4}$ fragment ions are associated with the metals binding at the reducing terminus, the branching mannose, and the non-reducing terminus of the glycan structure, respectively. Therefore, these three positions on the glycan represent the most favored metal-binding sites. Based on the QE distributions (Fig. 1), the transition metals Mn^{2+}, Ni^{2+}, and the alkaline earth metal Mg^{2+} are associated with all three binding sites, although the relative preferences for each metal are different. In contrast, the transition metals Fe^{2+}, Co^{2+}, and Cu^{2+} bind almost exclusively to the branching mannose and the non-reducing terminus. The alkaline earth metals Ca^{2+} and Ba^{2+} are primarily located at the reducing terminus. We envision that these specific binding preferences could be potentially used to control fragmentation patterns of isomeric glycans with the goal of maximizing detection of diagnostic ions that can discriminate between structural isomers.

Comparison of the Source Distributions with QE Distributions

Figure 1 demonstrates that the source and QE distributions share many aspects in common. They show the same cross-section range for each glycan ion, and the features from both distributions differ only in their relative abundances. For instance, the features that have the cross section ranges of conformers *I* and *III* from the source distribution of $[Man_5GlcNAc_2 + Mn]^{2+}$ both decrease in intensities upon activation. As a result, conformer *II*, which is of low abundance in the source distribution, becomes the most intense feature. In contrast, for the Ca^{2+} adducted glycan, conformer *II* is not observed from the QE distribution, while it appears to be the second most abundant conformation in the source distribution. Overall, the activation process causes a decrease of certain

features and increase of others. We suggest that the different features from the source distributions are also associated with different metal-binding positions on the glycan.

Although it is still controversial whether structural populations of a molecule change when it transitions from solution into the gas phase, several studies on proteins [57, 85, 86] and peptides [68] suggested that when ionized using gentle conditions, the gas-phase ion population is an appropriate reflection of their solution states. We therefore posit that our observed source distribution likely reflects the underlying solution phase population, whereas the QE distribution represents the population of the energy favored gas-phase conformations. To estimate the relative abundances of conformations in the source distribution of a given metal ion, we divided each overall distribution into the three conformational ranges based on those from the QE distributions (Fig. 1). Table 1 shows the relative abundances of the metal ions at the three major binding sites for both the source and QE distributions. In the case of Ba^{2+}, the values are not listed because they may not represent the actual ion populations for reasons discussed above. For the transition metals as well as Mg^{2+}, more than half of the population is located at the non-reducing terminus in the source distributions. This preference is highest for Co^{2+}, in which 81% is bound to this site. These transition metals bind poorly to the reducing terminus, except for Mn^{2+}, Ni^{2+}, and Mg^{2+}, which have slightly higher probability of binding there. When Ca^{2+} binds to the glycan, the most stable location is at the reducing terminus for both the QE and the source distributions.

Summary and Conclusions

We have characterized a series of metal ions complexed to the glycan $Man_5GlcNAc_2$ by IMS and MS/MS analyses. IMS distributions demonstrated that the metallated ions for this glycan display a range of distinct structural conformations. Such a diversity largely results from the metal ions binding a number of different sites on the glycan. The distictive distribution of IMS conformations indicates that each metal has a preferential pattern of binding sites. MS/MS fragmentaion of each metal-glycan ion gives three predominant product ions: B_4, $Y_{3\alpha}$, and $Y_{3,4}$. These fragments enabled us to localize the metal ion to specific regions of the glycan structure. A correlation is found between the QE distributions and the MS/MS fragmentation patterns of the glycan ions. That is, the QE distributions of glycan conformations likely represent the distributions of conformers from which the fragment ions are formed. Specifically, the conformers *I*, *II*, and *III* in the QE distributions represent the conformations that produce the CID fragments B_4, $Y_{3\alpha}$, and $Y_{3,4}$, respectively. For transition metals, the source distribution conformations are more likely to have metals bound to the non-reducing terminus, whereas the QE conformations bind to both the non-reducing terminus and the branching site except for Ni^{2+}, which binds to the three sites with similar affinity. The alkaline earth metals Ca^{2+} and Ba^{2+} prefer binding to the reducing terminus in both distributions.

The QE distribution bridges between the source distribution and the MS/MS fragmentation pattern of the glycan ion and represents the population of conformers prior to fragmentation, whereas the source distributions are likely to be associated with metal-specific conformations in solution.

Acknowledgments

References

1. Helenius, A.: Intracellular functions of N-linked glycans. Science **291**, 2364–2369 (2001)
2. Dwek, R.A.: Glycobiology: toward understanding the function of sugars. Chem. Rev. **96**, 683–720 (1996)
3. Varki, A.: Biological roles of oligosaccharides: all of the theories are correct. Glycobiology **3**, 97–130 (1993)
4. Thu, B., Skjåk-Bræk, G., Micali, F., Vittur, F., Rizzo, R.: The spatial distribution of calcium in alginate gel beads analysed by synchrotron-radiation induced X-ray Emission (SRIXE). Carbohydr. Res. **297**, 101–105 (1997)
5. Müthing, J., Maurer, U., Weber-Schürholz, S.: Glycosphingolipids of skeletal muscle: II. Modulation of Ca^{2+}-flux in triad membranes by gangliosides. Carbohydr. Res. **307**, 147–157 (1998)
6. Hartinger, C.G., Nazarov, A.A., Ashraf, S.M., Dyson, P.J., Keppler, B.K.: Carbohydrate–metal complexes and their potential as anticancer agents. Curr. Med. Chem. **15**, 2574–2591 (2008)
7. Gyurcsik, B., Nagy, L.: Carbohydrates as ligands: coordination equilibria and structure of the metal complexes. Coord. Chem. Rev. **203**, 81–149 (2000)
8. Fenn, J.B., Mann, M., Meng, C.K., Wong, S.F., Whitehouse, C.M.: Electrospray ionization for mass spectrometry of large biomolecules. Science **246**, 64–71 (1989)
9. Han, L., Costello, C.: Mass spectrometry of glycans. Biochem. Mosc. **78**, 710–720 (2013)
10. Zaia, J.: Mass spectrometry of oligosaccharides. Mass Spectrom. Rev. **23**, 161–227 (2004)
11. Stumpo, K.A., Reinhold, V.N.: The N-Glycome of Human Plasma. J. Proteome Res. **9**, 4823–4830 (2010)
12. Harvey, D.J.: Analysis of carbohydrates and glycoconjugates by matrix-assisted laser desorption/ionization mass spectrometry: an update for 2007–2008. Mass Spectrom. Rev. **31**, 183–311 (2012)
13. Medzihradszky, K.F., Gillece-Castro, B.L., Townsend, R.R., Burlingame, A.L., Hardy, M.R.: Structural elucidation of O-linked glycopeptides by high energy collision-induced dissociation. J. Am. Soc. Mass Spectrom. **7**, 319–328 (1996)
14. Prien, J.M., Ashline, D.J., Lapadula, A.J., Zhang, H., Reinhold, V.N.: The high mannose glycans from bovine ribonuclease B isomer characterization by ion trap MS. J. Am. Soc. Mass Spectrom. **20**, 539–556 (2009)
15. Costello, C.E., Contado-Miller, J.M., Cipollo, J.F.: A glycomics platform for the analysis of permethylated oligosaccharide alditols. J. Am. Soc. Mass Spectrom. **18**, 1799–1812 (2007)
16. Harvey, D.J.: Collision-induced fragmentation of underivatized N-linked carbohydrates ionized by electrospray. J. Mass Spectrom. **35**, 1178–1190 (2000)
17. Harvey, D.J.: Ionization and collision-induced fragmentation of N-linked and related carbohydrates using divalent cations. J. Am. Soc. Mass Spectrom. **12**, 926–937 (2001)
18. Cancilla, M.T., Penn, S.G., Carroll, J.A., Lebrilla, C.B.: Coordination of alkali metals to oligosaccharides dictates fragmentation behavior in matrix assisted laser desorption ionization/Fourier transform mass spectrometry. J. Am. Chem. Soc. **118**, 6736–6745 (1996)
19. Sible, E.M., Brimmer, S.P., Leary, J.A.: Interaction of first row transition metals with α1–3, α1–6 mannotriose and conserved trimannosyl core oligosaccharides: a comparative electrospray ionization study of doubly and singly charged complexes. J. Am. Soc. Mass Spectrom. **8**, 32–42 (1997)
20. Yu, X., Huang, Y., Lin, C., Costello, C.E.: Energy-dependent electron activated dissociation of metal-adducted permethylated oligosaccharides. Anal. Chem. **84**, 7487–7494 (2012)
21. Bohrer, B.C., Merenbloom, S.I., Koeniger, S.L., Hilderbrand, A.E., Clemmer, D.E.: Biomolecule analysis by ion mobility spectrometry. Annu. Rev. Anal. Chem. **1**, 293–327 (2008)
22. Tang, K., Li, F., Shvartsburg, A.A., Strittmatter, E.F., Smith, R.D.: Two-dimensional gas-phase separations coupled to mass spectrometry for analysis of complex mixtures. Anal. Chem. **77**, 6381–6388 (2005)
23. Kanu, A.B., Dwivedi, P., Tam, M., Matz, L., Hill, H.H.: Ion mobility-mass spectrometry. J. Mass Spectrom. **43**, 1–22 (2008)
24. Shvartsburg, A.A., Li, F., Tang, K., Smith, R.D.: Characterizing the structures and folding of free proteins using 2-D gas-phase separations: observation of multiple unfolded conformers. Anal. Chem. **78**, 3304–3315 (2006)
25. Ruotolo, B.T., Verbeck, G.F., Thomson, L.M., Gillig, K.J., Russell, D.H.: Observation of conserved solution-phase secondary structure in gas-phase tryptic peptides. J. Am. Chem. Soc. **124**, 4214–4215 (2002)
26. Williams, J.P., Grabenauer, M., Holland, R.J., Carpenter, C.J., Wormald, M.R., Giles, K., Harvey, D.J., Bateman, R.H., Scrivens, J.H., Bowers, M.T.: Characterization of simple isomeric oligosaccharides and the rapid separation of glycan mixtures by ion mobility mass spectrometry. Int. J. Mass Spectrom. **298**, 119–127 (2010)
27. Harvey, D.J., Scarff, C.A., Edgeworth, M., Crispin, M., Scanlan, C.N., Sobott, F., Allman, S., Baruah, K., Pritchard, L., Scrivens, J.H.: Traveling wave ion mobility and negative ion fragmentation for the structural determination of N-linked glycans. Electrophoresis **34**, 2368–2378 (2013)
28. Zhu, M., Bendiak, B., Clowers, B., Hill, H.H.: Ion mobility mass spectrometry analysis of isomeric carbohydrate precursor ions. Anal. Bioanal. Chem. **394**, 1853–1867 (2009)
29. Dwivedi, P., Bendiak, B., Clowers, B.H., Hill, H.H.: Rapid resolution of carbohydrate isomers by electrospray ionization ambient pressure ion mobility spectrometry-time-of-flight mass spectrometry (ESI-APIMS-TOFMS). J. Am. Soc. Mass Spectrom. **18**, 1163–1175 (2007)
30. Both, P., Green, A., Gray, C., Šardzík, R., Voglmeir, J., Fontana, C., Austeri, M., Rejzek, M., Richardson, D., Field, R., Widmalm, G., Flitsch, S.L., Eyers, C.E.: Discrimination of epimeric glycans and glycopeptides using IM-MS and its potential for carbohydrate sequencing. Nat. Chem. **6**, 65–74 (2014)
31. In, L., Barran, P.E., Deakin, J.A., Lyon, M., Uhrin, D.: Conformation of glycosaminoglycans by ion mobility mass spectrometry and molecular modelling. Phys. Chem. Chem. Phys. **7**, 3464–3471 (2005)
32. Olivova, P., Chen, W., Chakraborty, A.B.., Gebler, J.C.: Determination of N-glycosylation sites and site heterogeneity in a monoclonal antibody by electrospray quadrupole ion-mobility time-of-flight mass spectrometry. Rapid Commun. Mass Spectrom. **22**, 29–40 (2008)
33. Vakhrushev, S.Y., Langridge, J., Campuzano, I., Hughes, C., Peter-Katalinić, J.: Ion mobility mass spectrometry analysis of human glycourinome. Anal. Chem. **80**, 2506–2513 (2008)
34. Seo, Y., Andaya, A., Leary, J.A.: Preparation, separation, and conformational analysis of differentially sulfated heparin octasaccharide isomers using ion mobility mass spectrometry. Anal. Chem. **84**, 2416–2423 (2012)
35. Kailemia, M., Park, M., Kaplan, D., Venot, A., Boons, G.-J., Li, L., Linhardt, R., Amster, I.J.: High-field asymmetric-waveform ion mobility spectrometry and electron detachment dissociation of isobaric mixtures of glycosaminoglycans. J. Am. Soc. Mass Spectrom. **25**, 258–268 (2014)
36. Huang, Y., Dodds, E.D.: Ion mobility studies of carbohydrates as group I adducts: isomer-specific collisional cross section dependence on metal ion radius. Anal. Chem. **85**, 9728–9735 (2013)
37. Fenn, L.S., McLean, J.A.: Structural resolution of carbohydrate positional and structural isomers based on gas-phase ion mobility mass spectrometry. Phys. Chem. Chem. Phys. **13**, 2196–2205 (2011)
38. Hoffmann, W., Hofmann, J., Pagel, K.: Energy-resolved ion mobility-mass spectrometry—a concept to improve the separation of isomeric carbohydrates. J. Am. Soc. Mass Spectrom. **25**, 471–479 (2014)
39. Lee, S., Valentine, S.J., Reilly, J.P., Clemmer, D.E.: Analyzing a mixture of disaccharides by IMS-VUVPD-MS. Int. J. Mass Spectrom. **309**, 161–167 (2012)
40. Zhu, F., Lee, S., Valentine, S., Reilly, J., Clemmer, D.: Mannose7 glycan isomer characterization by IMS-MS/MS analysis. J. Am. Soc. Mass Spectrom. **23**, 2158–2166 (2012)

41. Plasencia, M.D., Merenbloom, S.I., Mechref, Y., Clemmer, D.E.: Resolving and assigning N-Linked glycan structural isomers from ovalbumin by IMS-MS. J. Am. Soc. Mass Spectrom. **19**, 1706–1715 (2008)

42. Koeniger, S.L., Merenbloom, S.I., Valentine, S.J., Jarrold, M.F., Udseth, H.R., Smith, R.D., Clemmer, D.E.: An IMS-IMS analogue of MS-MS. Anal. Chem. **78**, 4161–4174 (2006)

43. Pierson, N.A., Valentine, S.J., Clemmer, D.E.: Evidence for a quasi-equilibrium distribution of states for bradykinin M+3H (3+) ions in the gas phase. J. Phys. Chem. B **114**, 7777–7783 (2010)

44. Pierson, N.A., Clemmer, D.E.: An IMS-IMS threshold method for semi-quantitative determination of activation barriers: interconversion of proline Cis↔Trans forms in triply protonated bradykinin. Int. J. Mass Spectrom. (2014). doi:10.1016/j.ijms.2014.07.012

45. Glover, M.S., Dilger, J.M., Zhu, F., Clemmer, D.E.: The Binding of Ca^{2+}, Co^{2+}, Ni^{2+}, Cu^{2+}, and Zn^{2+} cations to angiotensin I determined by mass spectrometry-based techniques. Int. J. Mass Spectrom. **354–355**, 318–325 (2013)

46. Liang, C.J., Yamashita, K., Kobota, A.: Structure study of carbohydrate moiety from bovine pancreas ribonuclease B. J. Biochem. **88**, 51–58 (1980)

47. Fu, D.T., Chen, L., Oneill, R.A.: A detailed structure characterization of ribonuclease B oligosacchrides by H^1NMR sepctroscopy and mass spectrometry. Carbohydr. Res. **261**, 173–186 (1994)

48. Revercomb, H.E., Mason, E.A.: Theory of plasma chromatography/gaseous electrophoresis. Review. Anal. Chem. **47**, 970–983 (1975)

49. Mesleh, M.F., Hunter, J.M., Shvartsburg, A.A., Schatz, G.C., Jarrold, M.F.: Structural information from ion mobility measurements: effects of the long-range potential. J. Phys. Chem. **100**, 16082–16086 (1996)

50. Shvartsburg, A.A., Jarrold, M.F.: An exact hard-spheres scattering model for the mobilities of polyatomic ions. Chem. Phys. Lett. **261**, 86–91 (1996)

51. St. Louis, R.H., Hill, H.H., Eiceman, G.A.: Ion mobility spectrometry in analytical chemistry. Crit. Rev. Anal. Chem. **21**, 321–355 (1990)

52. Hoaglund-Hyzer, C.S., Counterman, A.E., Clemmer, D.E.: Anhydrous protein ions. Chem. Rev. **99**, 3037–3080 (1999)

53. von Helden, G., Wyttenbach, T., Bowers, M.T.: Conformation of macro-molecules in the gas phase: use of matrix-assisted laser desorption methods in ion chromatography. Science **267**, 1483–1485 (1995)

54. Hoaglund, C.S., Valentine, S.J., Sporleder, C.R., Reilly, J.P., Clemmer, D.E.: Three-dimensional ion mobility TOFMS analysis of electrosprayed biomolecules. Anal. Chem. **70**, 2236–2242 (1998)

55. Clemmer, D.E., Jarrold, M.: Ion mobility measurements and their applications to clusters and biomolecules. J. Mass Spectrom. **32**, 577–592 (1997)

56. Isailovic, D., Plasencia, M.D., Gaye, M.M., Stokes, S.T., Kurulugama, R.T., Pungpapong, V., Zhang, M., Kyselova, Z., Goldman, R., Mechref, Y., Novotny, M.V., Clemmer, D.E.: Delineating diseases by IMS-MS profiling of serum N-linked glycans. J. Proteome Res. **11**, 576–585 (2012)

57. Shi, H.L., Pierson, N.A., Valentine, S.J., Clemmer, D.E.: Conformation types of ubiquitin M+8H (8+) ions from water: methanol solutions: evidence for the N and A states in aqueous solution. J. Phys. Chem. B **116**, 3344–3352 (2012)

58. Merenbloom, S.I., Koeniger, S.L., Valentine, S.J., Plasencia, M.D., Clemmer, D.E.: IMS-IMS and IMS-IMS-IMS/MS for separating peptide and protein fragment ions. Anal. Chem. **78**, 802–2809 (2006)

59. Tang, K., Shvartsburg, A.A., Lee, H.-N., Prior, D.C., Buschbach, M.A., Li, F., Tolmachev, A.V., Anderson, G.A., Smith, R.D.: High-sensitivity ion mobility spectrometry/mass spectrometry using electrodynamic ion funnel interfaces. Anal. Chem. **77**, 3330–3339 (2005)

60. Mirza, U.A., Chait, B.T.: Do proteins denature during droplet evolution in electrospray ionization? Int. J. Mass Spectrom. Ion Process. **162**, 173–181 (1997)

61. Loo, R.R.O., Smith, R.D.: Investigation of the gas-phase structure of electrosprayed proteins using ion-molecule reactions. J. Am. Soc. Mass Spectrom. **5**, 207–220 (1994)

62. Covey, T., Douglas, D.J.: Collision cross sections for protein ions. J. Am. Soc. Mass Spectrom. **4**, 616–623 (1993)

63. Li, J., Taraszka, J.A., Counterman, A.E., Clemmer, D.E.: Influence of solvent composition and capillary temperature on the conformations of electrosprayed ions: unfolding of compact ubiquitin conformers from pseudonative and denatured solutions. Int. J. Mass Spectrom. **185–187**, 37–47 (1999)

64. Suckau, D., Shi, Y., Beu, S.C., Senko, M.W., Quinn, J.P., Wampler, F.M., McLafferty, F.W.: Coexisting stable conformations of gaseous protein pons. Proc. Natl. Acad. Sci. U. S. A. **90**, 790–793 (1993)

65. Hudgins, R.R., Woenckhaus, J., Jarrold, M.F.: High resolution ion mobility measurements for gas phase proteins: correlation between solution phase and gas phase conformations. Int. J. Mass Spectrom. Ion Process. **165/166**, 497–507 (1997)

66. Loo, J.A., Loo, R.R.O., Udseth, H.R., Edmonds, C.G., Smith, R.D.: Solvent-induced conformational changes of polypeptides probed by electrospray-ionization mass spectrometry. Rapid Commun. Mass Spectrom. **5**, 101–105 (1991)

67. Katta, V., Chait, B.T.: Observation of the heme–globin complex in native myoglobin by electrospray-ionization mass spectrometry. J. Am. Chem. Soc. **113**, 8534–8535 (1991)

68. Pierson, N.A., Chen, L., Valentine, S.J., Russell, D.H., Clemmer, D.E.: Number of solution states of bradykinin from ion mobility and mass spectrometry measurements. J. Am. Chem. Soc. **133**, 13810–13813 (2011)

69. Zucker, S.M., Lee, S., Webber, N., Valentine, S.J., Reilly, J.P., Clemmer, D.E.: An ion mobility/ion trap/photodissociation instrument for characterization of ion structure. J. Am. Soc. Mass Spectrom. **22**, 1477–1485 (2011)

70. Lee, S., Li, Z.Y., Valentine, S.J., Zucker, S.M., Webber, N., Reilly, J.P., Clemmer, D.E.: Extracted fragment ion mobility distributions: a new method for complex mixture analysis. Int. J. Mass Spectrom. **309**, 154–160 (2012)

71. Kang, P., Mechref, Y., Klouckova, I., Novotny, M.V.: Solid-phase permethylation of glycans for mass spectrometric analysis. Rapid Commun. Mass Spectrom. **19**, 3421–3428 (2005)

72. Ceroni, A., Maass, K., Geyer, H., Geyer, R., Dell, A., Haslam, S.M.: GlycoWorkbench: a tool for the computer-assisted annotation of mass spectra of glycans. J. Proteome Res. **7**, 1650–1659 (2008)

73. Domon, B., Costello, C.E.: A systematic nomenclature for carbohydrate fragmentations in FAB-MS/MS spectra of glycoconjugates. Glycoconj. J. **5**, 397–409 (1988)

74. Williams, J.P., Brown, J.M., Campuzano, I., Sadler, P.J.: Identifying drug metallation sites on peptides using electron transfer dissociation (ETD), collision induced dissociation (CID), and ion mobility-mass spectrometry (IM-MS). Chem. Commun. **46**, 5458–5460 (2010)

75. Robinson, E.W., Leib, R.D., Williams, E.R.: The role of conformation on electron capture dissociation of ubiquitin. J. Am. Soc. Mass Spectrom. **17**, 1470–1480 (2006)

76. Devakumar, A., Thompson, M.S., Reilly, J.P.: Fragmentation of oligosaccharide ions with 157 nm vacuum ultraviolet light. Rapid Commun. Mass Spectrom. **19**, 2313–2320 (2005)

77. Stephens, E., Maslen, S.L., Green, L.G., Williams, D.H.: Fragmentation characteristics of neutral N-linked glycans using a MALDI-TOF/TOF tandem mass spectrometer. Anal. Chem. **76**, 2343–2354 (2004)

78. Harvey, D.J., Bateman, R.H., Green, M.R.: High-energy collision-induced fragmentation of complex oligosaccharides ionized by matrix-assisted laser desorption/ionization mass spectrometry. J. Mass Spectrom. **32**, 167–187 (1997)

79. Chen, X., Fung, Y.M.E., Chan, W.Y.K., Wong, P.S., Yeung, H.S., Chan, T.-W.D.: Transition metal ions: charge carriers that mediate the electron capture dissociation pathways of peptides. J. Am. Soc. Mass Spectrom. **22**, 2232–2245 (2011)

80. Grese, R.P., Cerny, R.L., Gross, M.L.: Metal ion-peptide interactions in the gas phase: a tandem mass spectrometry study of alkali metal cationized peptides. J. Am. Chem. Soc. **111**, 2835–2842 (1989)

81. Isailovic, D., Kurulugama, R.T., Plasencia, M.D., Stokes, S.T., Kyselova, Z., Goldman, R., Mechref, Y., Novotny, M.V., Clemmer, D.E.: Profiling of human serum glycans associated with liver cancer and cirrhosis by IMS-MS. J. Proteome Res. **7**, 1109–1117 (2008)

82. McLuckey, S.A.: Principles of collisional activation in analytical mass spectrometry. J. Am. Soc. Mass Spectrom. **3**, 599–614 (1992)

83. McLuckey, S.A., Goeringer, D.E.: Special feature: tutorial slow heating methods in tandem mass spectrometry. J. Mass Spectrom. **32**, 461–474 (1997)

84. Wells, J.M., McLuckey, S.A.: Collision-Induced Dissociation (CID) of Peptides and Proteins. In: Burlingame, A.L. (ed.) Methods in Enzymology, p. 148. Academic Press, Waltham (2005)

85. Wyttenbach, T., Pierson, N.A., Clemmer, D.E., Bowers, M.T.: Ion mobility analysis of molecular dynamics. Annu. Rev. Phys. Chem. **65**, 175–196 (2014)

86. Shi, H., Atlasevich, N., Merenbloom, S., Clemmer, D.: Solution dependence of the collisional activation of ubiquitin [M + 7H]7+ ions. J. Am. Soc. Mass Spectrom. (2014) doi:10.1007/s13361-014-0834-y